

Ice conditions for maritime traffic in the Baltic Sea in future climate

Anders Höglund, Per Pemberton, Robinson Hordoir and Semjon Schimanke

Swedish Meteorological and Hydrological Institute, S-601 76 Norrköping, Sweden

Received 29 July 2016, final version received 15 Mar. 2017, accepted 27 Mar. 2017

Höglund A., Pemberton P., Hordoir R. & Schimanke S. 2017: Ice conditions for maritime traffic in the Baltic Sea in future climate. *Boreal Env. Res.* 22: 245–265.

Ice conditions for maritime traffic in the Baltic Sea in past/present (1961–2005) and future climates (2006–2100) were investigated. To model the ice conditions, a state-of-the-art ocean model, Nemo-Nordic, with a coupled ice model, LIM3, was applied. The model is forced with downscaled atmospheric fields from two global climate models using two different greenhouse-gas concentration scenarios giving an ensemble of four realisations of possible future ice conditions. Even though ice extent will be reduced in future climate and ice seasons will become shorter, completely ice-free winters are unlikely during the present century. In future climate, the ice becomes thinner, thus fewer traffic restrictions will be needed, but with a large inter-annual variability. In future climate, the ice will also become more mobile.

Background

The Baltic Sea is a semi-closed sea in northern Europe (Fig. 1). It is one of the heaviest navigated seas in the world with about 15% of the world's cargo transportation occurring there (HELCOM 2009). During winter, large parts of the Baltic Sea are covered with sea ice, which severely affects maritime traffic and requires ice breaking services.

The two most important factors affecting maritime traffic in winter are sea-ice extent and wind (BIM 2008). Sea-ice extent varies among years, causing some ports to be ice free during some winters, while they are ice infested during other winters. The wind and ocean currents cause ice motion and/or internal ice pressure, which can lead to ridging of sea ice. Ridges in the Baltic Sea may be as thick as 15 m (Lep-päranta and Myrberg 2009) and are of great

concern to maritime traffic. In addition, ice pressure can also severely hinder ice-going maritime traffic leading to assistance from icebreakers being required. Leads in the sea ice, which can occur due to a divergent ice field, or be created by ships, are frequently used as passage ways for maritime winter traffic. Ice motion may also close the leads made by e.g. icebreakers, sometimes directly after the icebreaker, requiring ships to go in convoy with an icebreaker or in extreme cases, be towed.

During the ice season, restrictions are imposed on maritime traffic for safety reasons (HELCOM 2004). These restrictions are based on the thickness of the fast ice. When restrictions are in effect, only ships with a high enough ice class can expect to receive icebreaking services. Ships are classified according to their ability to operate independently in ice conditions through certain technical requirements, for example by

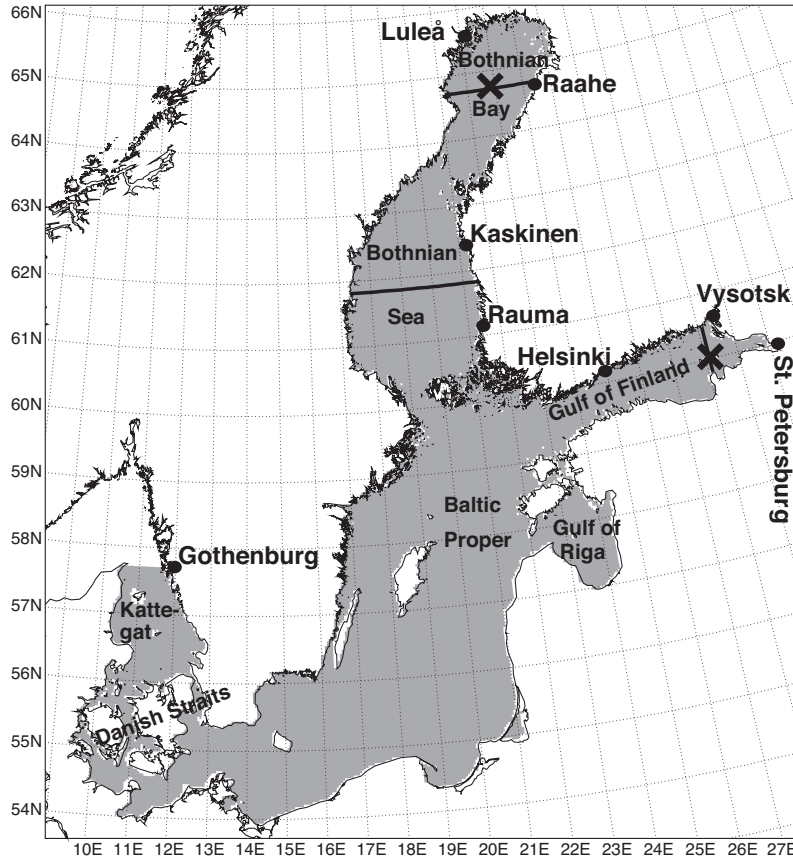


Fig. 1. The Baltic Sea computational domain (in grey). The crosses show the locations for which the changes in distribution of ice drift velocity is presented in the section “Sea-ice drift” and the lines show the sections for which the sea-ice drift and currents are illustrated.

specifying hull strength, engine power and propulsion machinery (TraFi 2010). The icebreaking authorities may impose additional conditions on minimum engine power, as well as granting exemptions during favourable weather conditions.

During the last two centuries, maximum ice extent in the Baltic Sea was steadily decreasing (Vihma and Haapala 2009). In future, milder winters are expected and consequently there will be less ice in the Baltic Sea. This is supported by all recent climate projection studies (e.g. Haapala *et al.* 2001, Meier 2006, Luomaranta *et al.* 2014). However, the climate projections also show that even for the most aggressive greenhouse-gas concentration scenario, the Baltic Sea is unlikely to be completely ice free during the 21st century (Luomaranta *et al.* 2014). The reduction in ice will be seen as reduced ice extent, reduced ice thickness and a shorter ice season (Vihma and Haapala 2009). This means that more ports can

be operated without maritime traffic restrictions for a longer part of the year, or even the whole year, while ports that still have restrictions may have lower restrictions.

Maritime winter navigation in the Baltic Sea has recently attracted attention of the safety and risk-management community. The focus is operational risk management (e.g. Boström and Österman 2016, Goerlandt *et al.* 2016), as well as strategic risk management (e.g. Valdez-Banda *et al.* 2015, 2016). The purpose of the present study is to provide this community with information on how climate change will affect parameters important for maritime winter navigation.

In this study, we show how the Baltic Sea ice will change in a future climate under different greenhouse-gas concentration scenarios. We used a state-of-the-art ice–ocean model which resolves ice thickness distribution, which had not been done in earlier studies, and thus provides information important to maritime traffic.

We focused on large-scale, regional and local changes.

Methods

Model

We used a coupled ice–ocean model system called Nemo-Nordic (Hordoir *et al.* 2013, 2015) which builds upon the model framework Nucleus for European Modelling of the Ocean (NEMO) ver. 3.6 (*see* <http://www.nemo-ocean.eu/>) and the integrated Louvain-la-Neuve sea-ice model (LIM3) (Vancoppenolle *et al.* 2009). Nemo-Nordic has been configured to simulate the ocean and sea-ice dynamics in the North Sea and Baltic Sea region on both short forecast time scales (hours to days) and long climate time scales (several decades up to hundreds of years). To save computing time, we used a restricted Baltic-only domain that covers the Baltic Sea and the Kattegat. As the effect of the North Sea state on the seasonal Baltic Sea ice cover is very modest, this regional limitation should not impose any large constraints on our results. The Baltic-only domain has the same horizontal and vertical grids as the full Nemo-Nordic configuration but with an open boundary in Kattegat instead of the Channel and North Sea. The horizontal resolution was 0.055° along the zonal axis, and 0.033° along the meridional axis, which corresponds to a nominal resolution of roughly two nautical miles (3704 m). The vertical resolution was 3 m in the upper layers, down to 60 m, and then gradually increased to 22 m at depth.

The LIM3 sea-ice component is a dynamic-thermodynamic sea-ice model with multi-layer halo-thermodynamics and a multi-category ice thickness distribution (Vancoppenolle *et al.* 2009, Rousset *et al.* 2015). For a detailed description of the LIM3 implementation within Nemo-Nordic *see* Appendix.

Simulations

Using an ensemble of experiments, we investigate how the sea-ice state in the Baltic Sea will evolve in future climate. This is achieved

by forcing Nemo-Nordic with the atmospheric fields from several different regional dynamical downscalings of the past, present and future Baltic climate using the regional atmospheric climate model RCA4 (Schimanke *et al.* 2014). In the downscalings, RCA4 was forced at its lateral boundaries by two different global climate models (GCM): EC-Earth and MPI. For each GCM case, a historical simulation also referred to as the control simulation, covering the period 1961–2005, and two Representative Concentration Pathways scenarios (RCP4.5 and RCP8.5) covering the period 2006–2100 was carried out. Table 1 summarises the set-ups for the different simulations. To evaluate the quality of the different GCM cases, we compared the historical simulations with a hindcast simulation for the same period. In the hindcast simulation, Nemo-Nordic was forced by a downscaling of the ERA-40 reanalysis data set (Kupiainen *et al.* 2011). All simulations were started from a rest state with salinity and temperature as climatological values. Along the open boundary in Kattegat the model was forced by sea-level variations using the method described in Meier *et al.* (2012). The method used sea-level pressure from an RCA4 simulation, forced by the ERA-40 reanalysis on the lateral boundary, to estimate the sea level variability along the boundary. To further increase the quality of the variability, the data were bias corrected using tide gauge measurements from Gothenburg. For temperature and salinity on the boundary and runoff into the Baltic Sea we used climatological values. Previous studies (e.g., Meier *et al.* 2012) demonstrated that there is no use implementing a

Table 1. List of simulations.

Simulation	Period	GCM	Scenario/ forcing
Hindcast	1961–2006		ERA-40
MPI			
historical	1961–2005	MPI	Historical
RCP4.5	2006–2100	MPI	RCP4.5
RCP8.5	2006–2100	MPI	RCP8.5
EC-Earth			
historical	1961–2005	EC-Earth	Historical
RCP4.5	2006–2100	EC-Earth	RCP4.5
RCP8.5	2006–2100	EC-Earth	RCP8.5

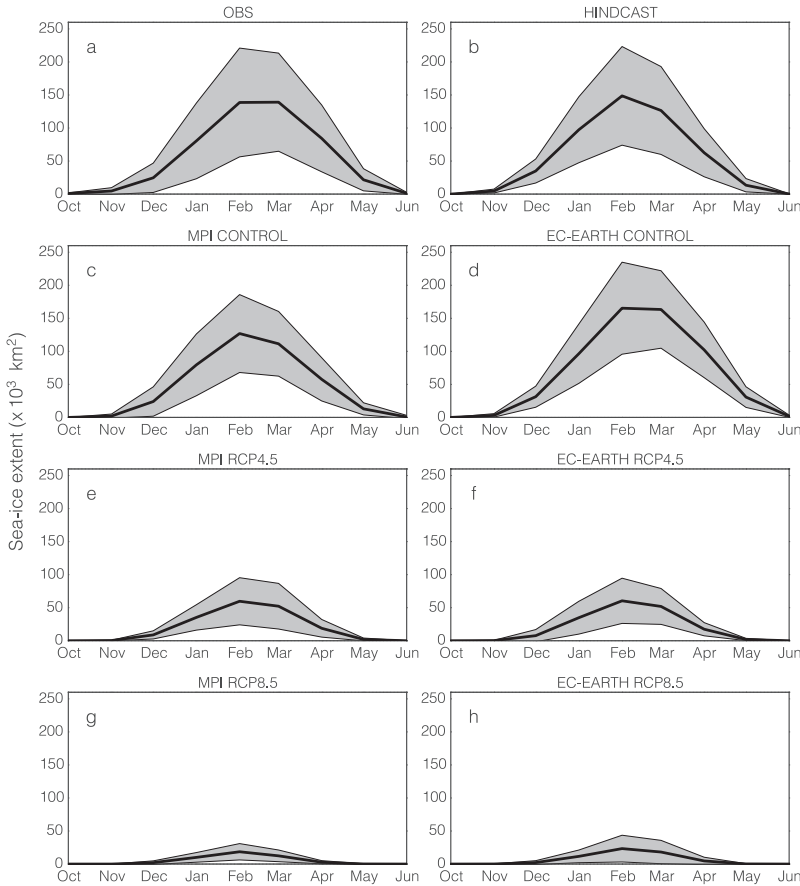


Fig. 2. Long-term monthly Baltic Sea sea-ice extent \pm SD (grey).

boundary condition that takes the climate change signal into account for temperature, as most of the temperature trend in a Baltic Sea model comes from the atmospheric forcing.

To evaluate the historical simulations we also used ice concentration from a set of near weekly ice charts from the Ice Service at the Swedish Meteorological and Hydrological Institute. For a more thorough evaluation of the Nemo-Nordic sea-ice component *see* Appendix.

Results

Here we present the large scale and local changes in the Baltic Sea ice extent, thickness, deformation, drift and length of season as they all show how climate change affects the Baltic Sea ice, and are relevant parameters for planning of future maritime winter navigation. We focus

on the changes occurring between a historical (1970–1999) and a future (2070–2099) periods.

Sea-ice extent and thickness

The sea-ice extent was calculated as the area where sea-ice concentration is at least 15%. It is evident that sea-ice extent in Nemo-Nordic agreed well with the observations and that the EC-Earth driven runs generally indicated more ice than the MPI driven runs for the 1970–1999 period (Fig. 2). In the RCP4.5 scenario, the February mean ice extent is reduced by 63% and 53% in the EC-Earth driven and MPI driven cases, respectively; while the more aggressive RCP8.5 scenarios show a reduction of 86% and 85%, respectively.

For the period 1970–1999, the EC-Earth driven run has on average a yearly maximum ice

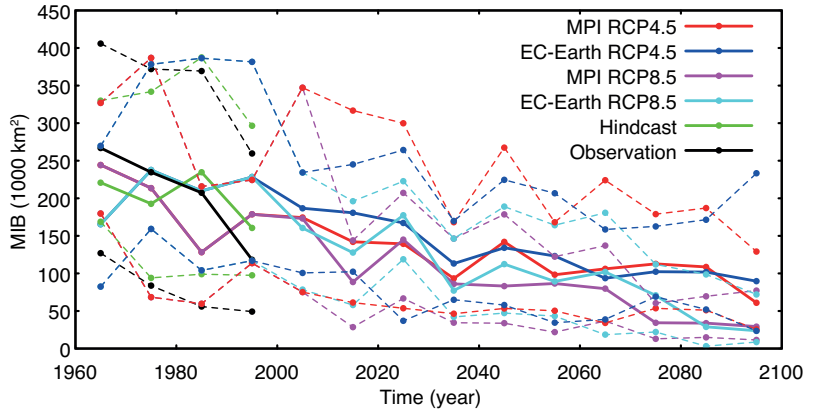


Fig. 3. Decadal means (solid), minima and maxima (dashed) of the annual maximum ice extent of the Baltic Sea.

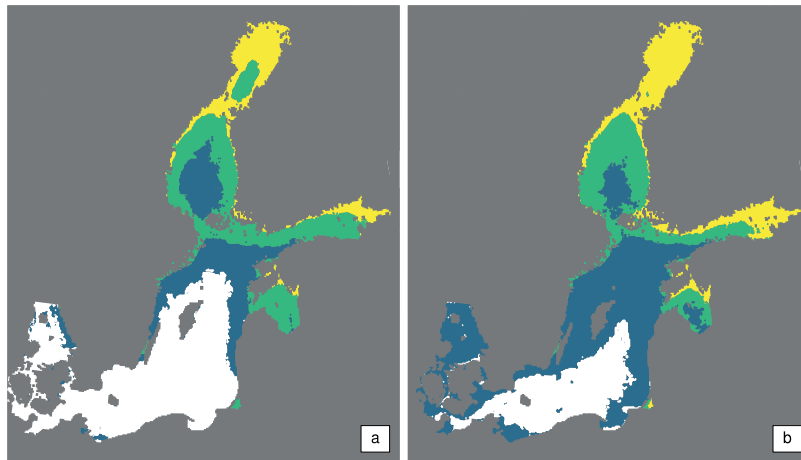


Fig. 4. Long-term mean of the annual maximum ice extent for (a) MPI and (b) EC-Earth driven scenarios. The yellow, yellow/green and yellow/green/blue areas show the coverage for the RCP8.5, RCP4.5 and historical scenarios, respectively. The RCP4.5 and RCP8.5 scenarios are averaged for 2070–2099 and the historical simulations for 1970–1999.

extent of 225 000 km and the MPI driven run 173 000 km (Fig. 3). The hindcast run and the observations are in the midst with 196 000 km and 187 000 km respectively. For the period 2070–2099 in the RCP8.5 scenarios, the proportions in the EC-Earth driven simulation and the MPI driven one are about the same as for the earlier period, 41 000 km and 32 000 km respectively. However, in the RCP4.5 scenarios they are practically the same, 98 000 km and 94 000 km respectively, due to the stronger reduction in the EC-Earth driven case. The trends in annual maximum sea-ice extent are 10 000, 11 000, 15 000, 15 000 km/decade for MPI RCP4.5, EC-Earth RCP4.5, MPI RCP8.5 and EC-Earth RCP8.5 cases, respectively. The trends were calculated using the decadal means for the entire 1961–2100 period. We note that considering high decadal variability, the period

for which the hindcast simulation is available is too short to let us say if it has similar climate.

For the period 1970–1999, EC-Earth gives a higher ice coverage in the Kattegat, Danish Straits, northern and southeastern parts of the Baltic Proper (Fig. 4). In the RCP4.5 scenarios, on average most of the ice coverage is lost in the Baltic Proper, Danish Straits and Kattegat in the period 2070–2099. The stronger reduction in EC-Earth for the 21st century yields a similar maximum ice extent for both RCP4.5 scenarios, however, the EC-Earth driven case gives a slightly higher coverage in the central Bothnian Sea and a lower coverage in the Gulf of Riga. For the RCP8.5 scenarios, there is a further loss of ice coverage in the Bothnian Sea, Gulf of Finland and Gulf of Riga. The MPI driven case gives on average a somewhat lower coverage in the Bothnian Sea and Gulf of Finland.

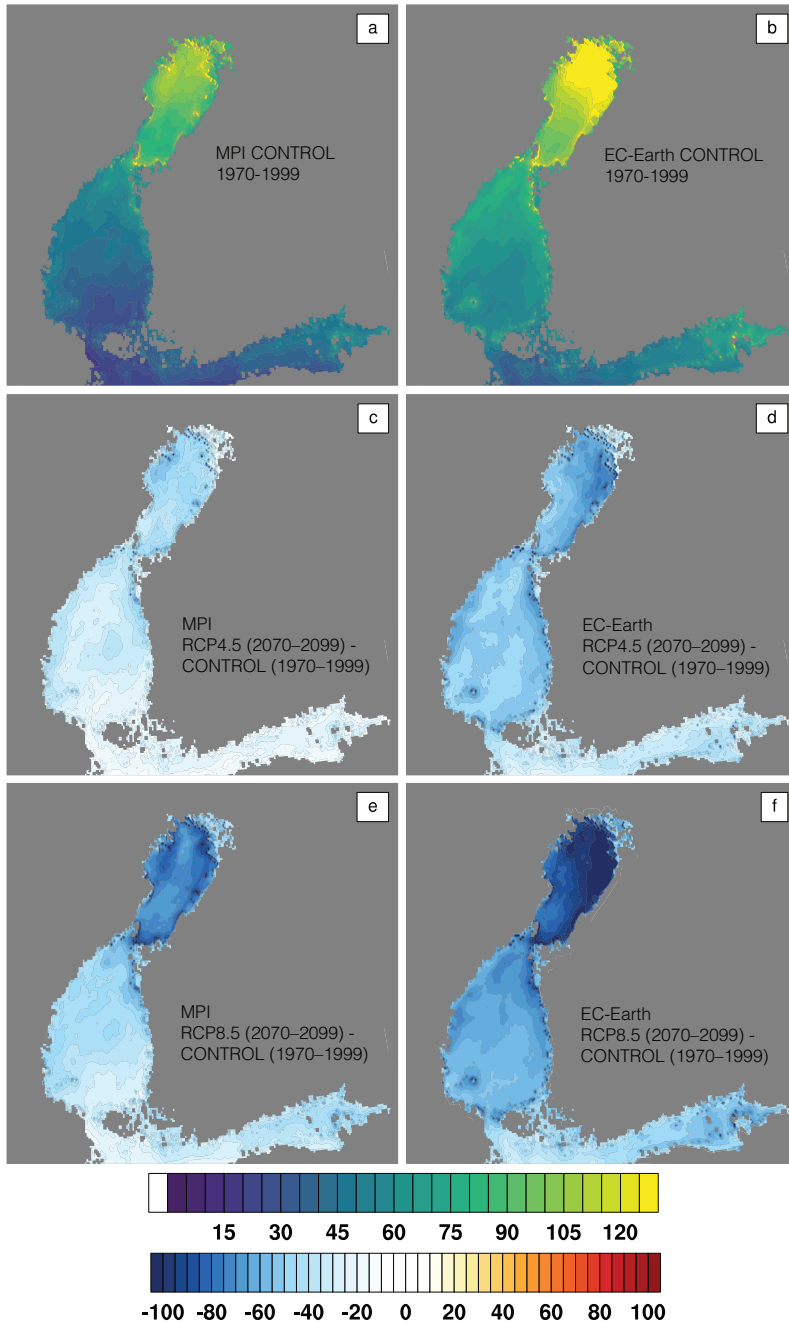
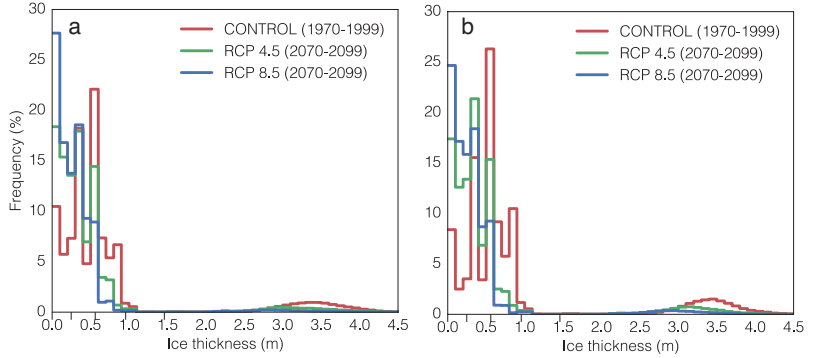


Fig. 5. Long-term means of annual maximum cell-averaged ice thickness for the (a) MPI and (b) EC-Earth driven historical simulations, and (d-f) differences between the historical simulations and different scenarios. The means are calculated for 1970–1999 and 2070–2099 for the historical and scenarios, respectively. The cell-averaged ice thickness is calculated as an ice concentration weighted mean of the ice thickness in each ice category.

Similar to ice extent, it is clear that the annual maximum sea-ice thickness is generally greater in the EC-Earth driven historical simulation, especially in the Bothnian Bay (Fig. 5). In addition, the ice thickness reduction in both RCP scenarios is greater in the EC-Earth simulations and is especially pronounced in regions where the ice is

thicker. For the northern port (Luleå), the trends are stronger in the EC-Earth scenarios for both RCP cases leading to similar ice thicknesses given by the MPI and EC-Earth driven scenarios, due to the thicker ice in the EC-Earth historical simulation (Table 2). On the other hand, in the southeastern ports (Helsinki and Vysotsk), the trends given

Fig. 6. March sea-ice thickness distributions, computed for the entire Bothnian Bay for (a) the MPI driven simulations and (b) the EC-Earth driven simulations. The tick marks along the x-axis show the thickness of the category bounds.



by the MPI and EC-Earth driven simulations are similar, leading to thinner ice especially in the MPI driven RCP8.5 scenario.

To study changes in the ice thickness distribution we focused on long-term mean March ice thickness distribution in the Bothnian Bay. The Bothnian Bay is the most heavily ridged part of the Baltic Sea, and the ice thickness range is greatest and the ice season longest there. This is also the most difficult area for ships to navigate during winter. The ice-thickness distributions for the Bothnian Sea and Gulf of Finland show similar features except that there is generally less deformed ice in those regions (not shown). We calculated the ice thickness distribution from sea-ice thickness in the different ice categories by computing the frequency of ice in a certain thickness interval, using the ice concentration of that category as weight. All the ice-thickness distributions follow a bimodal distribution (Fig. 6). For the historical period the main peak is centred around 0.6 m and covers the range 0.0–1.0 m. This is the range where in the Baltic Sea it

would be expected to find thermodynamically grown ice. The second peak, centred around 3.5 m, which is slightly more pronounced in the EC-Earth historical simulation, shows the occurrence of dynamically formed (ridged) ice. Thus the thickest (5th) ice category could be used as a proxy for ridged ice. For the different scenarios, representing future climate, the ice thickness distributions shift towards thinner ice with, as expected, the RCP8.5 outcome more extremely shifted than the RCP4.5 one. The ridging peak is much reduced in both scenarios for both GCM cases, however, the distributions show that there will still be ridged ice in the Bothnian Bay by the end of the 21st century. From the thickness distributions we could calculate a mean thickness by multiplying the mid-thickness of a bin with the respective frequency and then summing over all ice thickness bins. This yield mean thicknesses of 75 and 89 cm, averaged for the control period, for the MPI and EC-Earth driven scenarios, respectively. For the future period (2070–2099), the mean thickness given by RCP4.5

Table 2. Mean annual maximum ice thickness (cm) and trends (cm/decade) for three ports. The ice thicknesses are calculated from the cell-averaged ice thickness.

Model/scenario	Period	Luleå		Helsinki		Vysotsk	
		mean	trend	mean	trend	mean	trend
Hindcast	1970–1999	83		38		59	
MPI	1970–1999	85		34		61	
EC-Earth	1970–1999	98		45		73	
MPI RCP4.5	2070–2099	57	–3	17	–2	44	–2
EC-Earth RCP4.5	2070–2099	58	–4	18	–2	45	–2
MPI RCP8.5	2070–2099	33	–5	2	–3	19	–4
EC-Earth RCP8.5	2070–2099	33	–6	5	–3	26	–4

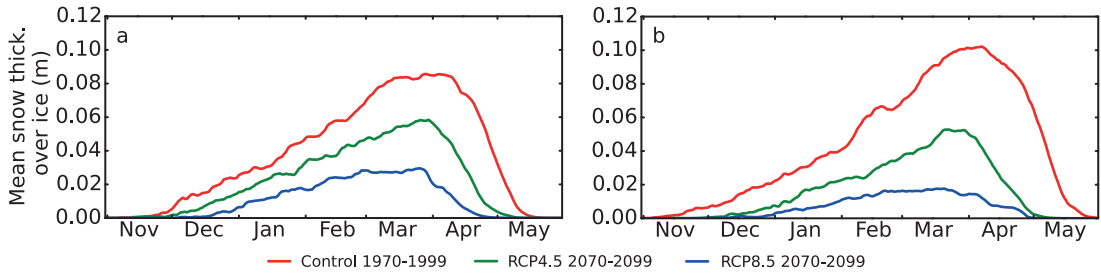


Fig. 7. Climatological mean snow cover on sea ice. (a) MPI-driven runs, and (b) EC-Earth driven runs.

(RCP8.5) is reduced to 47 (32) cm and 51 (36) cm for the MPI and EC-Earth cases, respectively. We noted that for the two GCM cases the reduction of the mean thickness calculated over the entire Bothnian Bay happened at the same rate as the one for Luleå, with a stronger reduction in EC-Earth driven scenarios.

Snow-cover and snow-fall changes

We computed the changes in mean snow-cover on sea ice, and the changes in mean snowfall onto ice for the whole computational domain. We found a maximum decrease in snow cover of 48% and 82% for the EC-Earth driven scenarios for the RCP4.5 and RCP8.5 scenarios, respectively (Fig. 7). We can associate this decrease with the total amount of snowfall on sea ice, which decreases by 48% and 76% for the RCP4.5 and RCP8.5 scenarios, respectively, rather than with the length of the ice season. The decrease in snowfall over the entire domain was higher and reached 62% and 79%.

For the MPI driven simulations, the decrease in snow thickness reached 31% and 65% for the RCP4.5 and RCP8.5 scenarios, respectively, which also fits with a total decrease in snowfall of 30% and 60%, respectively. For the entire domain, this decrease was higher by 42% and 75%, respectively.

Sea-ice drift

Here, we only consider model data from locations and times with at least 15% ice concentration and 0.1 m ice thickness. The focus is on the change of ice drift between the control period

(1970–1999) and the future period (2070–2099) within the climate runs. The reason is that the hindcast run shows lower ice drift velocities than the two climate runs during the control period. The average ice drift in the period 1970–1999 at a section through Bothnian Bay (*see* Fig. 1 for the location) has its maximum approximately in the centre of the section. For the hindcast, the largest value is 4.8 cm s^{-1} . For the MPI-driven simulation the largest value is 7.4 cm s^{-1} , i.e. 55% more. The EC-Earth driven simulations largest value is 6.2 cm s^{-1} , i.e. 29% more.

The Bothnian Bay will still be ice covered in future winters. In the section shown in Fig. 8 the minimum number of occurrences of ice for any single location for the RCP8.5 scenarios is 135 for the MPI driven run and 231 for the EC-Earth driven run. For the RCP4.5 scenarios the numbers are 1582 and 1497 respectively and for the control period 3050 and 3896 respectively.

The ice drift increases in the future (Fig. 8) and more so in the RCP8.5 scenario than in the RCP4.5 scenario. Close to the fast ice zone, the increase is from a very low level and thus shows a big increase in percent even though the increase is still at a low level. In the central part of the basin the increase in currents are close to the increase in ice drift.

The Bothnian Sea is normally not ice-covered in the central regions in the future period (Fig. 4). The ice drift increases in the regions that remain ice covered (Fig. 9) as do the currents. The increase in ice drift matches well with the increase in currents.

The Gulf of Finland is the only place where we see a reduction of ice drift. In the entrance area in the EC-Earth driven run of the RCP8.5 scenario there is an area with reduced ice drift by as much as 26%. This is an area with high ice

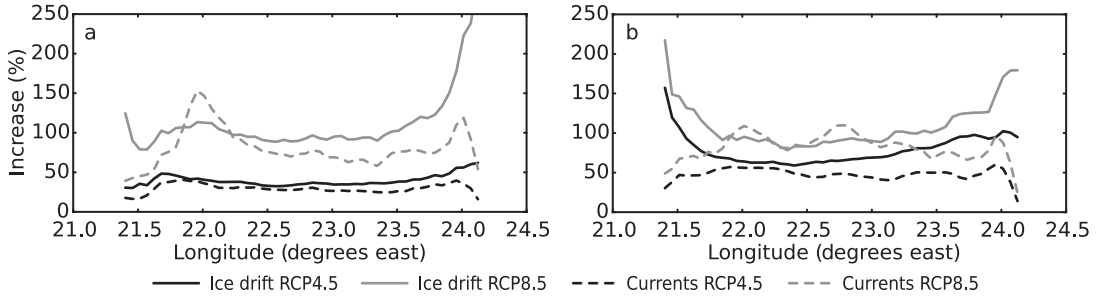


Fig. 8. Increase in ice drift and current velocity in the Bothnian Bay section at 64.72°N. Only occasions with at least 15% ice concentration and 0.1 m ice thickness are included for both ice drift and currents. (a) MPI-driven runs, and (b) EC-Earth-driven runs.

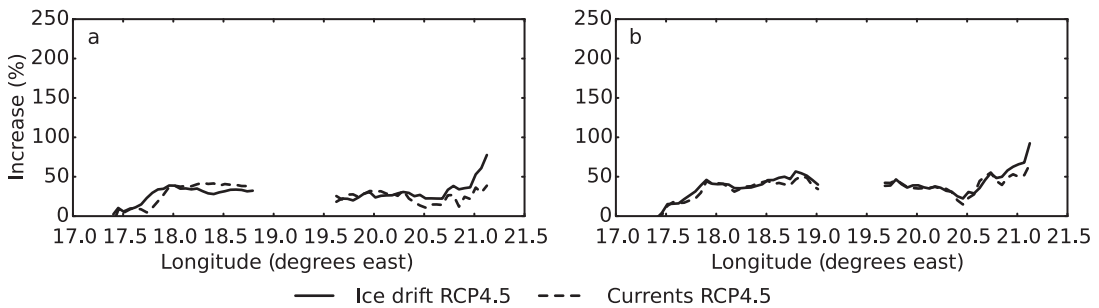


Fig. 9. Same as Fig. 8 but for the Bothnian Sea section at 61.82°N. The RCP8.5 scenarios contained too few occasions (< 50 per location) with ice, hence they were left out. The middle section of the RCP4.5 scenarios was left out for the same reason. (a) MPI-driven runs, and (b) EC-Earth-driven runs.

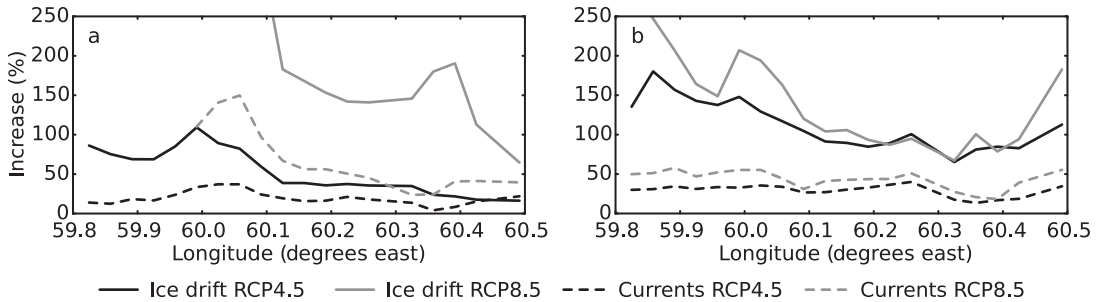


Fig. 10. Same as Fig. 8 but for the Gulf of Finland section at 28.12°E. The graphs for the RCP8.5 scenario in the MPI-driven run have been left out for the South due to too low sample sizes (< 50 occurrences with ice per location). (a) MPI-driven runs, and (b) EC-Earth-driven runs.

drift already in the control period and the number of occurrences with ice just above our limit of 50 occasions per position to be considered.

In the Gulf of Finland, there is also an agreement between an increase of ice drift and an increase of currents, although not as remarkable as in the Bothnian Sea. In the easternmost parts of the Gulf of Finland the agreement disappears (Fig. 10).

The distribution of velocities varies with the distance to the coast (Fig. 11). The location considered in the Gulf of Finland is close to the fast ice zone and representative of such locations. The ice is therefore less mobile with a high number of very low velocities compared with those in other locations. The RCP8.5 scenario for the MPI driven run was based on only 60 occurrences as compared with 298 occurrences for the EC-Earth

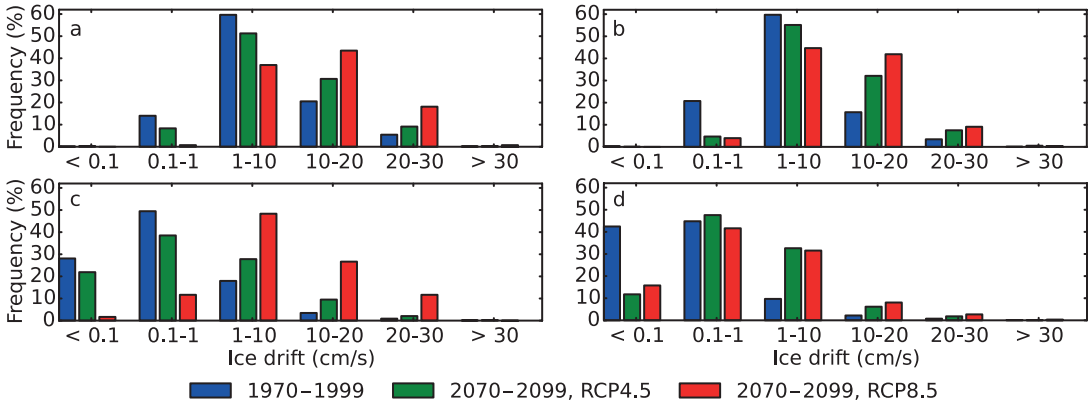


Fig. 11. Ice drift velocity frequencies for the Bothnian Bay (64.72°N, 22.79°E) (a) MPI-driven run, and (b) EC-Earth-driven run; as well as for the Gulf of Finland (59.99°N, 28.12°E) (c) MPI-driven run, and (d) EC-Earth-driven run (see Fig. 1 for the locations).

driven run. Some caution is therefore required in interpreting the apparent extreme number of higher velocities for this case. The location in the Bothnian Bay is more central in the basin and has very few occurrences of low velocities.

We did not see any change in magnitude of the higher velocities. This suggests some caution in interpreting the results as increased mobility and is further discussed in the discussion and conclusions section.

We found only small changes in the wind speed (not shown). The changes are generally below ten percent and the sign varies throughout the domain.

Sea-ice deformation

To evaluate how the ridging might change in a future climate we used the ice concentration and thickness in the thickest category as a proxy for ridges in the Baltic Sea. As already shown in the ‘Sea-ice extent and thickness’ section, there is a distinct separation between dynamically and thermodynamically grown ice in the model just below the lower limit (1.46 m) of the thickest ice category. The thickest ice usually occurs in low concentrations per grid cell, however, sometimes the model artificially creates unrealistically thick ice at extremely low concentrations. To filter out the extreme ice thickness we use a cut-off concentration of 0.2%, below which ice is not considered in the analysis.

In the control simulations the highest concentration of thick sea ice was found in the central Bothnian Bay and the eastern part of Gulf of Finland (Figs. 12–13). We noted that this was in agreement with the ridge density distribution, a different but similar measure of ridges, that Löptien *et al.* (2013) found in both observations and model. In addition, similar to the sea-ice extent and cell-averaged thickness, the EC-Earth driven control simulation produced a greater coverage of thick ice with a more pronounced concentration maximum in the Bothnian Bay. For the RCP4.5 scenarios there was a strong reduction of thick ice by the end of the 21st century. Both GCM cases produced similar patterns with the thickest ice found along the rim of the northern part of the Bothnian Bay, just outside the fast ice zone. In fact, the ice thickness in this region was slightly thicker than in the control simulations. In RCP8.5, most of the very thick ice was gone except for the northeastern part of the Bothnian Bay.

Length of ice season

Examining the 30-year mean of the length of the ice season for the control period in the Bothnian Bay, we found the hindcast simulation in the middle between the MPI and the EC-Earth driven simulations (Table 3). In the other two basins, the hindcast simulation was very close to the MPI driven simulation. The spread was generally higher in the control runs than in

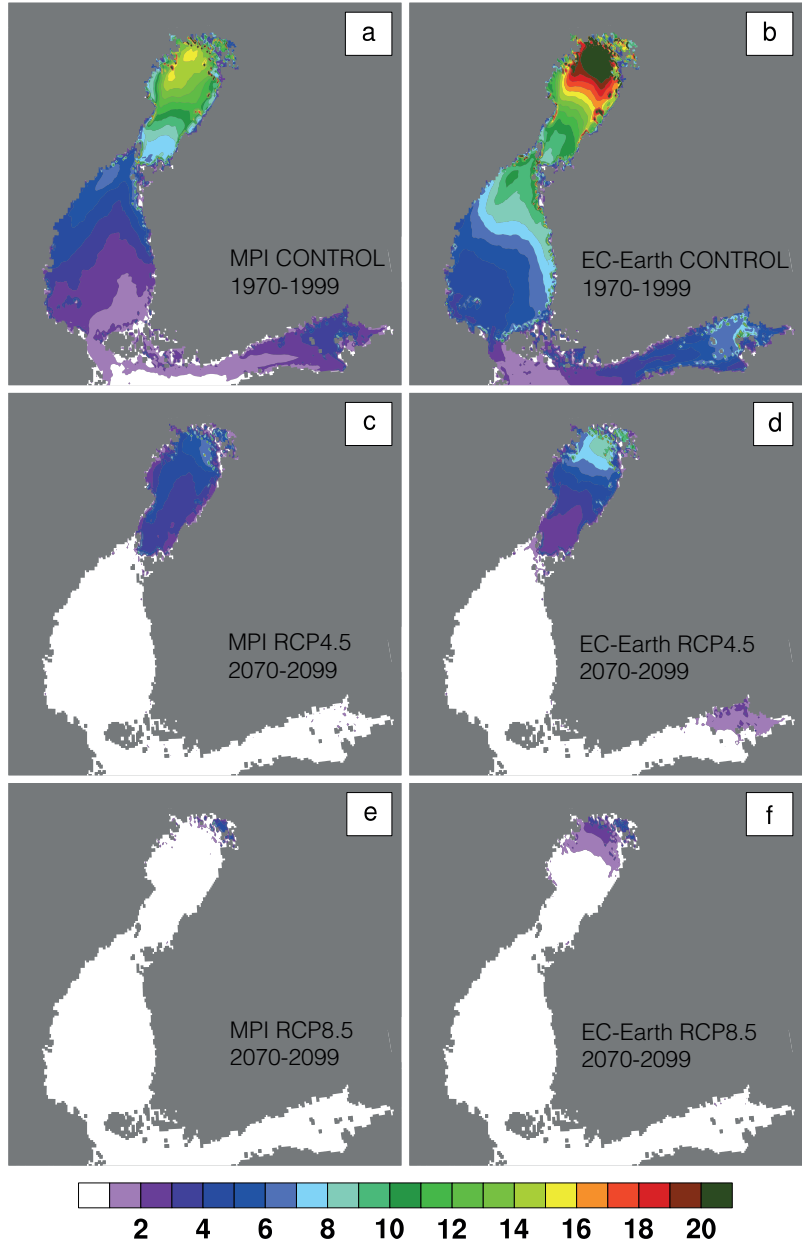


Fig. 12. Mean March–April sea-ice concentration (%) in category five for (a and b) control period, (c and d) RCP4.5 scenarios and (e and f) RCP8.5 scenarios.

the hindcast simulation, except for the Gulf of Finland, where they were very close and lower, respectively.

As the length of the ice season is changing over time, we chose to focus on the trends calculated via a least square fit of a line to the length of the ice season in respective basins. As a statistical measure of the uncertainty we used 95% confidence intervals (95%CI) of the trend. The

trend in length of the ice season for the hindcast simulation was within the confidence intervals of the control runs (Table 4). However, the 95%CIs were so wide that the sign of the trend for the hindcast could not be determined.

For the scenario period, the confidence intervals were narrower due to the longer time period. All the means + 95%CIs for the trends were still negative (Table 4) even though the values in

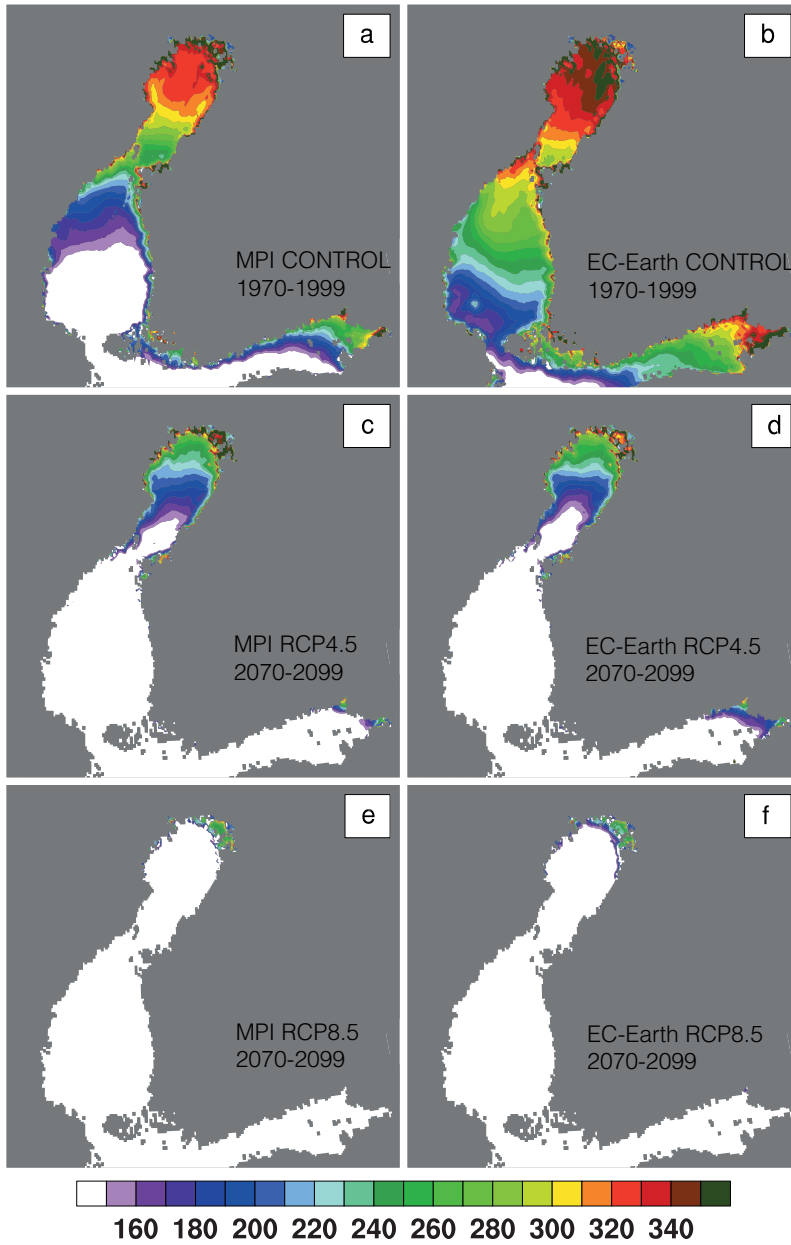


Fig. 13. Same as Fig. 12 but for sea-ice thickness (cm) in category five.

some cases were closer to zero than those for the control period. The trend in the break-up of the ice was stronger than the trend for the freezing (not shown) and thus contributed more to the change in the length of the ice season. The difference was consistent for all scenarios and basins. Assuming independence between the break up and freezing trends, we could calculate 95% CIs for the trend of the difference. For all but two of

the 12 scenario–basin combinations, the intervals excluded equality between the trends.

The magnitude of the trends was very different for the different scenarios, not only for RCP4.5 and RCP8.5 but also for the two global climate models for the same greenhouse-gas concentration scenarios, thus indicating a large uncertainty in the change of the length of the ice season.

For the historical period, the Gulf of Finland has the shortest ice season of the basins presented here. The trend is strongest for the Bothnian Sea and for the future period the Bothnian Sea has as short, or even shorter, ice season than in the Gulf of Finland.

Implications for maritime traffic restrictions

We examined the fast ice thicknesses close to the ports of Luleå (Fig. 14), Raahe, Kaskinen, Rauma, Helsinki (Fig. 15), Vysotsk (Fig. 16) and St. Petersburg. Those ports were chosen because they are of some importance, have a fast-ice zone in the model set-up and give a suitable distribution over the area.

For the control period, the MPI driven runs showed very good agreement with the hindcast for the two stations in the Bothnian Bay. The average the numbers of days per season with ice thickness 10 cm or more were 178.6 and 176.6 in the hindcast for Luleå and in the control run, respectively. For the thicknesses 15 cm, 30 cm, and 50 cm the numbers of days were on average 171.6, 144.1 and 103.9 days

for the hindcast, respectively, and 171.2, 145.9 and 108.9 days for the control run, respectively. For Raahe, the errors were -2.0 , -1.1 , -2.2 and -9.1 days. Continuing southwards, the sign of the errors become positive pointing to an 4–6-day overestimation of the number of days. In the Gulf of Finland, for the ports of Helsinki and St. Petersburg the errors were 6–9 days; for the two thicker classes for Helsinki, however, there was a slight underestimation. The greatest errors in the number of days was found for Vysotsk with about 10 days for the two lower classes and 13 days for the two higher classes.

The EC-Earth driven run produced a larger deviation with overestimation of the number of days for all location and classes. For the northerly locations the errors were about 10 days and for St. Petersburg about 20 days. Again the highest error with 23–24 days overestimation and as high as 27 days for the thickest ice class was found for Vysotsk. Helsinki was an exception with the errors of 12.6, 7.7, 2.0 and 0.8 days for the four ice thickness classes, respectively.

In the following we assume the current rules for traffic restrictions remain the same throughout the century. The ice thickness is strictly translated into the corresponding traffic restriction.

Table 3. Mean \pm SD length (days) of the ice season in different basins.

Model/scenario	Period	Bothnian Bay	Bothnian Sea	Gulf of Finland
Hindcast	1970–1999	215.7 \pm 9.6	186.7 \pm 11.8	172.4 \pm 15.4
MPI	1970–1999	205.0 \pm 14.6	184.7 \pm 19.0	178.4 \pm 15.6
EC-Earth	1970–1999	225.1 \pm 12.7	208.8 \pm 18.5	192.3 \pm 11.3
MPI RCP4.5	2070–2099	181.1 \pm 14.4	156.6 \pm 16.9	155.8 \pm 13.6
EC-Earth RCP4.5	2070–2099	177.6 \pm 15.3	152.1 \pm 17.2	156.8 \pm 16.4
MPI RCP8.5	2070–2099	145.3 \pm 17.0	113.2 \pm 22.7	114.8 \pm 26.3
EC-Earth RCP8.5	2070–2099	146.1 \pm 22.9	117.1 \pm 26.4	125.5 \pm 29.4

Table 4. Trends in length (days per decade) of the ice season (\pm 95%CI) in different basins. The trends are calculated by least square fit of a line to the length of the ice seasons over the respective periods.

Model/scenario	Period	Bothnian Bay	Bothnian Sea	Gulf of Finland
Hindcast	1962–2006	-0.86 ± 2.70	-2.35 ± 3.27	-1.18 ± 3.44
MPI	1962–2005	-2.66 ± 3.64	-4.91 ± 4.57	-4.80 ± 3.93
EC-Earth	1962–2005	-2.71 ± 3.19	-0.64 ± 4.37	-0.99 ± 2.74
MPI RCP4.5	2006–2099	-1.92 ± 1.00	-2.13 ± 1.24	-1.31 ± 1.04
EC-Earth RCP4.5	2006–2099	-4.83 ± 1.17	-6.10 ± 1.45	-4.10 ± 1.27
MPI RCP8.5	2006–2099	-6.62 ± 1.18	-7.30 ± 1.55	-6.96 ± 1.57
EC-Earth RCP8.5	2006–2099	-8.81 ± 1.26	-9.71 ± 1.51	-7.49 ± 1.47

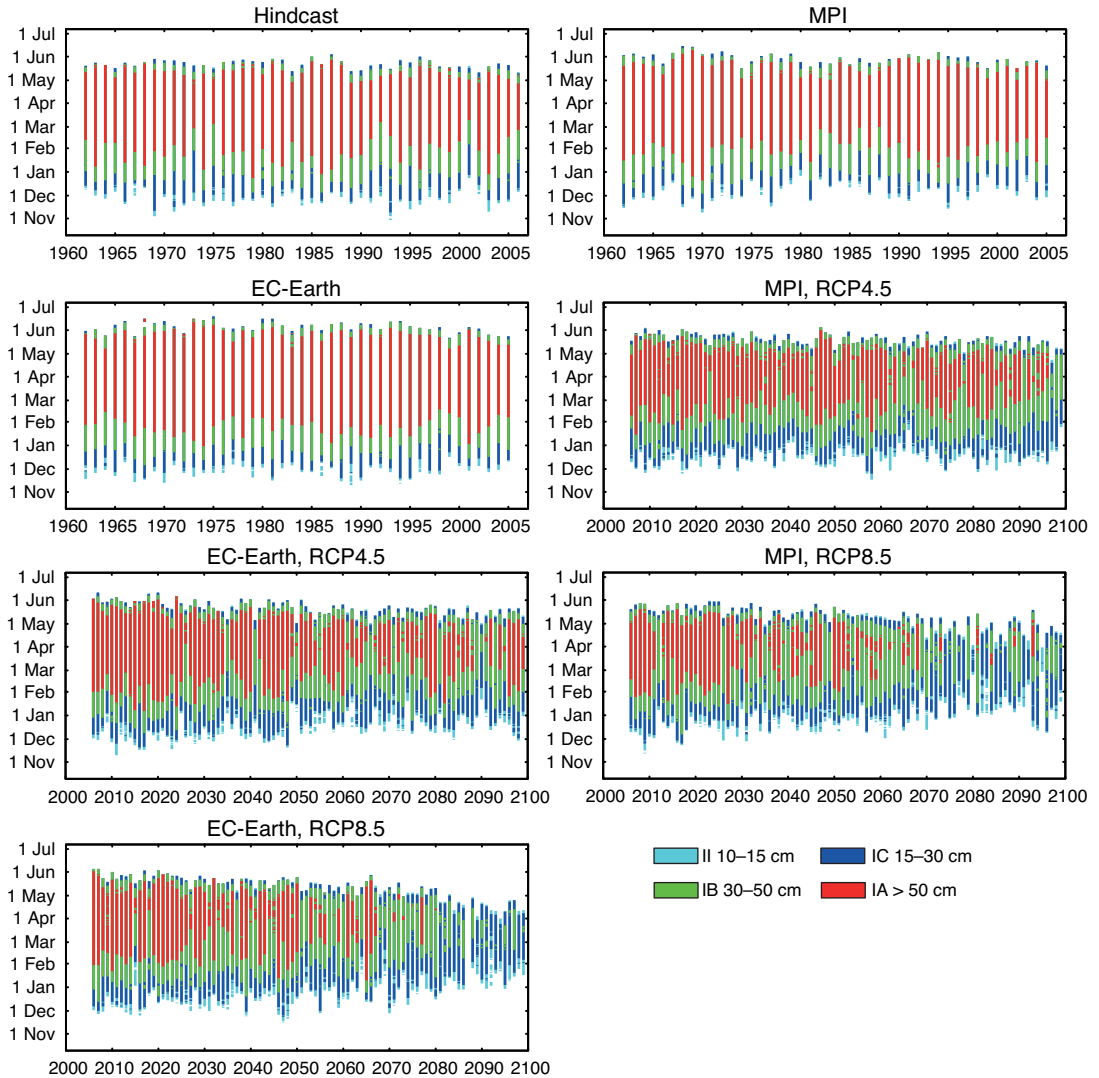


Fig. 14. Ice thickness of fast ice close to Luleå. The year 1962 refers to the ice season 1961–1962 etc. The limits of the colours are chosen to correspond to the ice classes in the Finnish–Swedish Ice Class Rules (TraFi 2010). Note that isolated events of thick ice at the end of, or after, the season are due to drifting ice entering the fast ice zone. The data have been slightly filtered for these events, but not all of them have been caught.

According to the RCP4.5 scenarios, at Luleå and Raahé there were 6 and 14 (MPI), and 11 and 8 (EC-Earth) seasons, respectively, when the traffic restrictions did not reach the highest level. In all those cases the second highest class was reached. In the RCP8.5 scenarios, there was one season in the EC-Earth driven simulation without traffic restrictions for Luleå and three for Raahé, while there were no seasons in the MPI driven simulations without traffic restrictions for

any of the ports. The highest ice class was rare at the end of the century (Fig. 14).

At Kaskinen there might already be seasons in the present climate when the highest ice class is not be reached. In the RCP4.5 scenarios there were seasons without restrictions. In the RCP8.5 scenarios there were several consecutive seasons without restrictions, but also seasons with long-lasting restrictions. In the MPI driven simulation, the first season without restrictions was already in

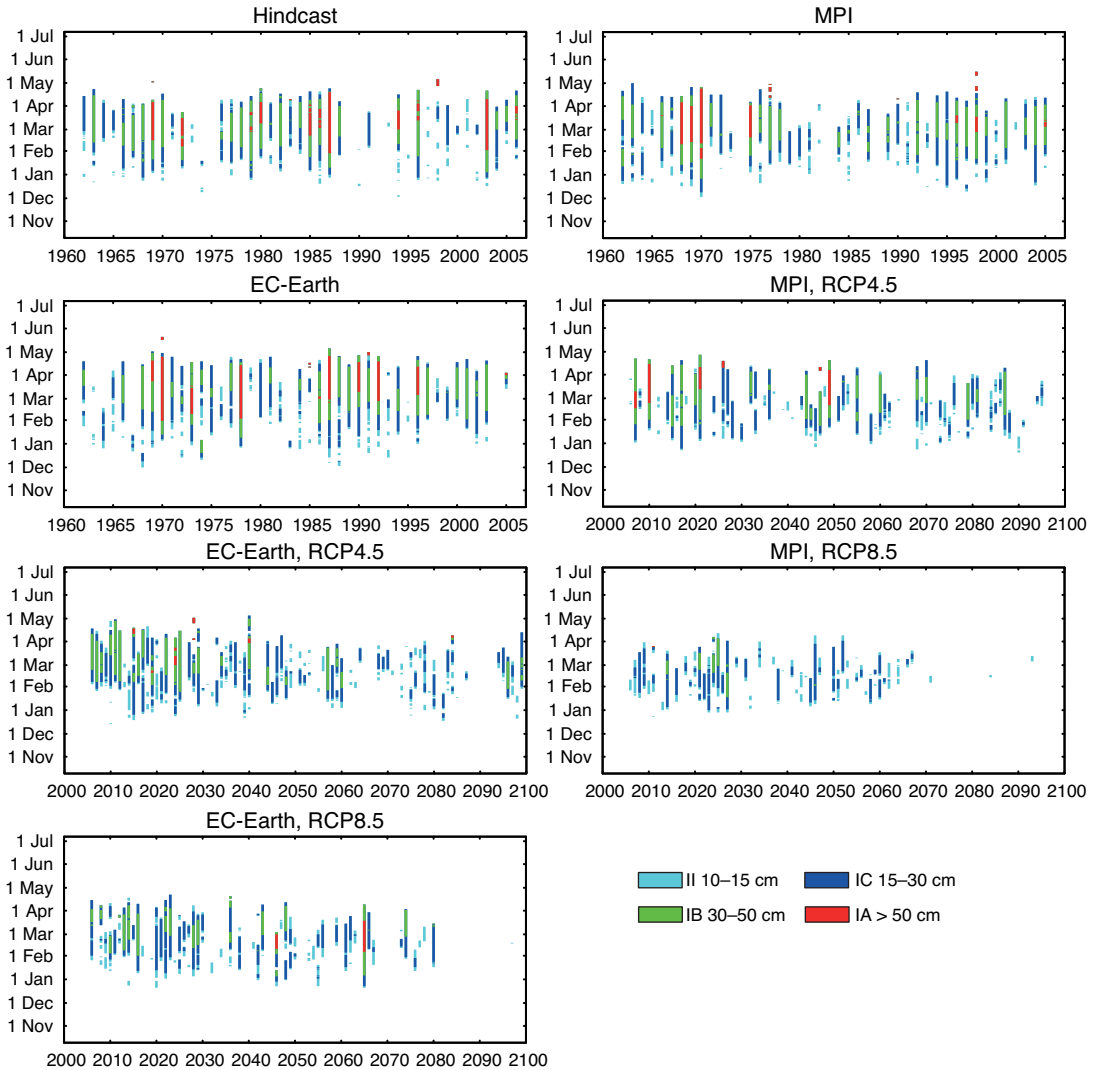


Fig. 15. Same as Fig. 14 but for fast ice close to Helsinki.

2012 but the next not until 2054. The first restriction-free season in the EC-Earth driven simulation was in 2069. There were, in total for the whole period, 13 seasons without traffic restrictions in each of the RCP8.5 scenarios. The highest ice class was very rare in the second half of the century. The last year with the highest class in the MPI driven simulation would be in 2066, lasting only for four days and in the EC-Earth driven simulation the two last ones would be in 2066 and 2073, and of 42 and 24 days length, respectively.

At Rauma there were restriction-free seasons already in the RCP4.5 scenarios, eight in the

MPI driven simulation and nine in the EC-Earth driven simulation. The highest ice class occurred, although very rarely by the end of the century. There were ten and five seasons in the second half of the century in the MPI driven simulation and EC-Earth driven simulation, respectively. In the RCP8.5 scenarios the majority of the seasons at the end of the century have no traffic restrictions. Of the last 20 years only six seasons in the MPI driven simulation and only three in the EC-Earth driven simulation had traffic restrictions.

Of the seven locations examined here, Helsinki has the least amount of ice, both in present

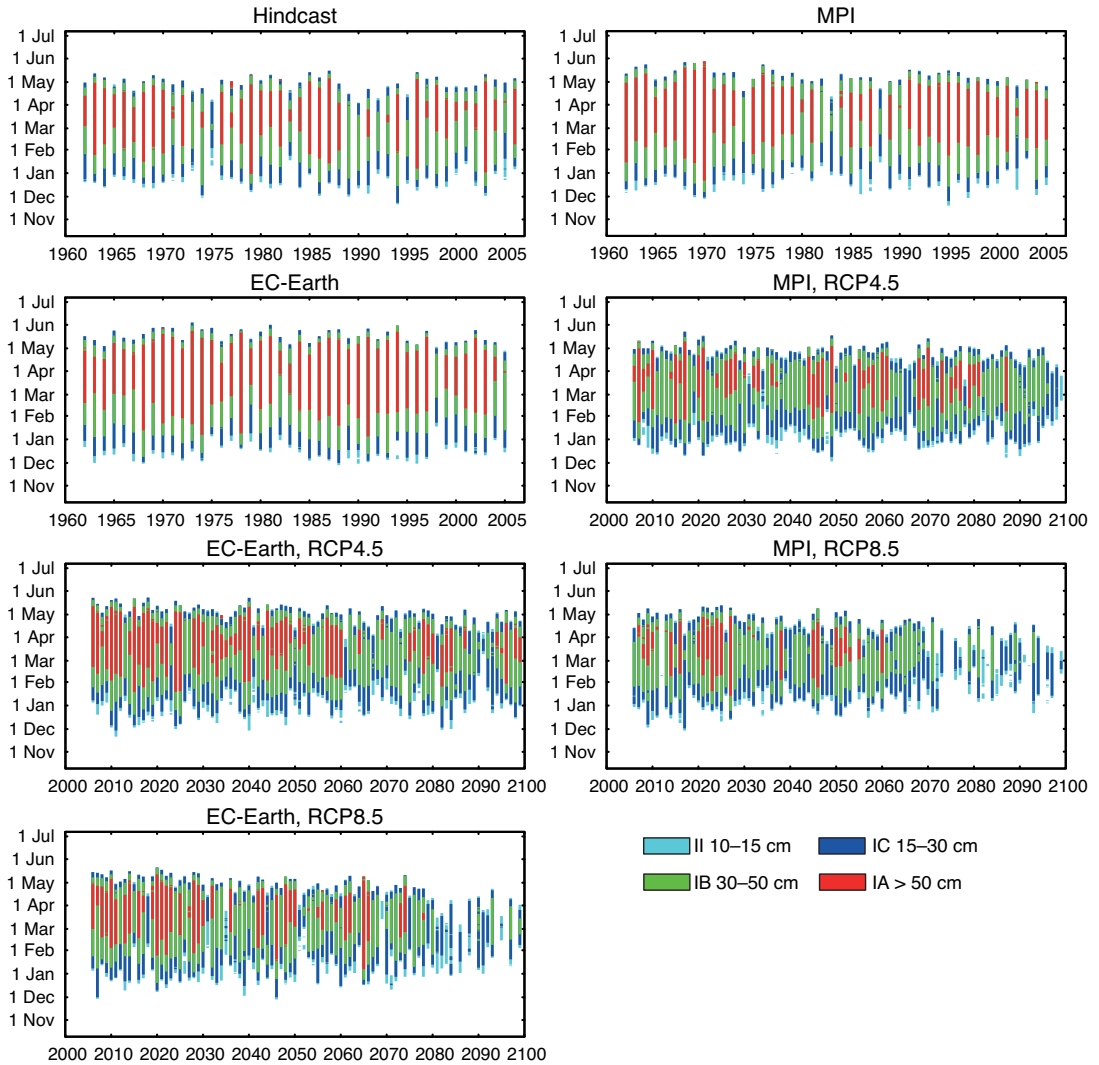


Fig. 16. Same as Fig. 14 but for fast ice close to Vysotsk.

climate and in the scenarios. There are already in the present climate consecutive seasons with no or almost no restrictions (Fig. 15). The highest ice class is unusual in present climate. In the RCP4.5 scenarios the highest ice class does almost not occur, only six seasons in each of the runs and many of the occasions in the EC-Earth simulation are only a few days long. In the RCP8.5 scenarios the highest ice class only occurs once in the MPI driven simulation and is only one day long. Since this is at the end of the season, it is probably drift ice the filtering failed to remove. In the EC-Earth scenario there are two occasions, 19 and 41 days long, with the

highest ice class. There are essentially no restrictions in the last 30 years in the MPI driven simulation and in the last 20 years in the EC-Earth driven simulation.

At Vysotsk (Fig. 16) and St. Petersburg there are no seasons without restrictions in the RCP4.5 scenarios. At St. Petersburg there is only one season where the second highest ice class is not reached (EC-Earth). At Vysotsk there are seven and three seasons where the second highest ice class is not reached in the MPI driven simulation and EC-Earth driven simulation, respectively. In the RCP8.5 scenario there are seasons without restrictions. For Vysotsk, there are six in each

simulation and for St. Petersburg there are two in the MPI driven simulation and one in EC-Earth driven simulation.

Discussion and conclusions

In the previous sections, we presented results comparing modelled ice for present climate, and of the future in two different greenhouse gas concentration scenarios (RCP4.5 and RCP8.5) and for each scenario, two different realisations (MPI and EC-Earth). The control period in the scenario runs was compared with a hindcast simulation or observations. We found that ice extent in the Nemo-Nordic model compares well to observations and that the control periods for the climate runs are on a par with the hindcast run for all parameters examined. Thus the climate scenarios capture the present climate well with respect to model biases and uncertainties. Our experiments also confirm previous findings (Haapala *et al.* 2001, Meier *et al.* 2004, Luomaranta *et al.* 2014) that wintertime sea ice will be present in the Baltic Sea even in the late 21st century.

In our study, the annual maximum sea ice extent was reduced by 46% and 57% for MPI and EC-Earth driven simulations, respectively, in the RCP4.5 scenario between the periods 1970–1999 and 2070–2099. This can be compared to the median value of 58% presented by Luomaranta *et al.* (2014) who used a much larger ensemble. For the RCP8.5 scenario, the corresponding values in our study are 81% and 82%, which are larger than the value of 74% found by Luomaranta *et al.* (2014). It should be noted that Luomaranta *et al.* (2014) did not use any ocean model but fitted an exponential function to observational values of maximum annual ice extent and atmospheric mean temperature for November–March. This means that the fitted function goes further outside the calibrated range for the more extreme scenario, which the authors note themselves, and therefore focuses their analysis on an earlier period.

Luomaranta *et al.* (2014) examined ice thickness in the fast ice zone. For the location of Kemi (close to Luleå), the trend for the RCP4.5 scenario was found to be -3.4 cm/decade and

for the RCP8.5 scenario to be -7.6 cm/decade. These values are close to those in Table 2 for the location of Luleå. Luomaranta *et al.* (2014) also looked at the location of Loviisa (between Helsinki and Vysotsk). There the trend was -3.3 cm/decade and -7.0 cm/decade for the RCP4.5 and RCP8.5 scenarios, respectively. These values are more negative than the values for Helsinki and Vysotsk in our study, especially for the RCP8.5 scenario. This is probably due to the difference in location. For Helsinki, many of the winters at the end of the century are ice free and thus the decreasing trend cannot continue. Loviisa is further to the east and will have some ice at the end of the century. Vysotsk, which is even further to the east, will have ice at the end of the century, thus the explanation used for Helsinki does not apply.

Increased ice mobility means that higher ice drift velocities become more common. At the same time, the extreme velocities are not higher in a future climate. It is not uncommon in today's climate, to find rather mobile ice in the beginning of the season and then again at the end of the season during melting. In the future climate, there is mobility throughout the shorter season.

All comparisons of ice drift in the present study was done for each grid cell in the model but only for locations with ice in the future period. Calculating the ice drift velocity averaged over the ice covered part of the whole model domain actually shows a reduction of the velocity in the future period for all scenarios. In the future period, many basins are ice free in the central regions where today's most mobile ice is found.

In the model data, we found no or little change in the wind but the currents under the ice increases nevertheless. With reduced ice extent in the future, the wind reaches more of the sea surface and thus causes higher currents during the ice season. This increase matches the increase in ice drift offshore.

For maritime winter navigation the occurrence of deformed ice either limits the traffic or requires additional assistance. As expected, our results show that the regions of heavily deformed ice will shrink (Figs. 12 and 13) and mostly occur in the Bothnian Bay, and only in coastal regions for the more aggressive RCP8.5

scenario. However, our results also show that we can still expect some thick ridges on average in the Bothnian Bay (Fig. 6). The main climate change signal is a decrease in the extent and thickness of the ice. This can lead to increased ice mobility and consequently more ridging events. Indeed our analysis shows an increase in ice drift, however, these changes do not produce any significant increases in ridged ice in our experiments, and are thus of second order.

The inter-annual variability of the ice climate is rather large. The span between the decadal minimum and maximum of ice extent in Fig. 3 is frequently more than five times the minimum value. Also, the variation in the decadal mean suggests that ten years is too short a period to average for this parameter. The 95% CIs in Table 4 for the historical period are so great that the sign of the trend cannot be determined in most cases, suggesting that even 44 years can be too short a period due to the large variability. Vihma and Haapala (2009) review many studies of the ice season length in the second half of the 20th century. Many studies found a trend but only some were significant. Vihma and Haapala (2009) also found that the trend is clearer for ice break-up than for the freezing, as seen in the present study.

Averaging over longer periods is not without problems due to the climate change trend. The standard deviations in Table 3 for the more aggressive greenhouse gas scenarios are probably strongly influenced by the trends (*see* Table 4).

The present study handled the large variability by analysing periods far apart in time, so that the climate signal is larger and the influence of errors due to the high variability is kept at an acceptable level. The largest uncertainty, however, is which greenhouse gas concentration scenario is the most likely one.

While the variability adds uncertainty to the results, it also has practical consequences. As can be seen in the results regarding traffic restrictions related to thickness of the fast ice (Figs. 14–16), there can be several consecutive winters with very little or no ice in a certain area followed by a long season with substantially more ice. This makes it difficult to plan ice breaker services, and to deal with expected demands to cut funding during long periods of

little or no ice. This concern is raised in BIM (2012). Another problem is how to train and maintain skills of icebreaker staff as mentioned in BIM (2008).

Boström and Österman (2016) interviewed personally officers on Swedish ice breakers and by means of questionnaires officers on merchant vessels calling northerly ports in the Baltic Sea. One of the findings was that experience in ice navigation and experience in receiving ice breaking assistance are important factors for safety. This was identified mainly as a problem for vessels originating from outside the Baltic Sea, that only occasionally visited ice infested waters. In a future climate with less ice, one could imagine this to be an issue already within the Baltic Sea for vessels only occasionally visiting northerly ports. This is especially a concern when considering the variability of the different ice seasons.

Finally, even though our findings are in line with many previous studies, the results need to be interpreted with some caution as they only represent one ocean-ice model and a relatively small ensemble of GCMs and RCP scenarios. To support future decision-making on wintertime maritime traffic, a larger multi-model ensemble would probably yield more robust results, and is thus proposed as a direction for future studies.

Acknowledgements: This work resulted from the BONUS Stormwinds project supported by BONUS (Art 185), funded jointly by the EU and the Swedish Research Council for Environment, Agriculture Sciences and Spatial Planning (FORMAS). This work was also funded by the SmartSea project of the Strategic Research Council of Academy of Finland, grant No: 292 985.

References

- BIM 2008. *Baltic Sea icebreaking report 2007–2008*. Baltic Icebreaking Management. [Available at <http://baltice.org/app/static/pdf/BIM%20Report%2007-08.pdf>].
- BIM 2012. *Baltic Sea Icebreaking Report 2011–2012*. Baltic Icebreaking Management. [Available at <http://baltice.org/app/static/pdf/BIM%20Report%2011-12.pdf>].
- Boström M. & Österman C. 2016. Improving operational safety during icebreaker operations. *WMU Journal of Maritime Affairs* 16: 73–88.
- Bouillon S., Morales Maqueda M., Legat V. & Fichefet T. 2009. An elastic-viscous-plastic sea ice model formulated on Arakawa B and C grids. *Ocean Modelling* 27:

- 174–184.
- Goerlandt F., Montewka J., Zhang W. & Kujala P. 2016. An analysis of ship escort and convoy operations in ice conditions. *Safety Science* 95: 198–209.
- Haapala J., Meier H.E.M. & Rinne J. 2001. Numerical Investigations of Future Ice Conditions in the Baltic Sea. *AMBIO* 30: 237–244.
- HELCOM 2004. *Recommendation 25/7 on safety of winter navigation in the Baltic Sea area*. Baltic Marine Environment Protection Commission (Helsinki Commission). [Available at <http://www.helcom.fi/Recommendations/Rec%2025-7.pdf>].
- HELCOM 2009. *Ensuring safe shipping in the Baltic*. Baltic Marine Environment Protection Commission (Helsinki Commission). [Available at <http://helcom.fi/Lists/Publications/Ensuring%20safe%20shipping%20in%20the%20Baltic.pdf>].
- Hordoir R., Dieterich C., Basu C., Dietze H. & Meier M. 2013. Freshwater outflow of the Baltic Sea and transport in the Norwegian current: A statistical correlation analysis based on a numerical experiment. *Continental Shelf Research* 64: 1–9.
- Hordoir R., Axell L., Löptien U., Dietze H. & Kuznetsov I. 2015. Influence of sea level rise on the dynamics of salt inflows in the baltic sea. *Journal of Geophysical Research: Oceans* 120: 6653–6668.
- Kupiainen M., Jansson C., Samuelsson P., Jones C., Willen U., Hansson U., Ullerstig A., Wang S. & Döscher R. 2011. *Rosby centre regional atmospheric model, RCA4*. Newsletter, Rosby Centre, SMHI. [Available at <http://www.smhi.se/en/Research/Research-departments/climate-research-rossby-centre2-552/1.16562>].
- Leppäranta M., & Myrberg K. 2009. *Physical oceanography of the Baltic Sea*. Springer, Berlin.
- Löptien U., Mårtensson S., Meier H.E.M. & Höglund A. 2013. Long-term characteristics of simulated ice deformation in the Baltic sea (1962–2007). *Journal of Geophysical Research: Oceans* 118: 801–815.
- Luomaranta A., Ruosteenoja K., Jylhä K., Gregow H., Haapala J. & Laaksonen A. 2014. Multimodel estimates of the changes in the Baltic Sea ice cover during the present century. *Tellus A*: 66, 22617, doi:10.3402/tellusa.v66.22617.
- Meier H.E.M., Döscher R. & Halkka A. 2004. Simulated distributions of Baltic Sea-ice in warming climate and consequences for the winter habitat of the Baltic ringed seal. *AMBIO* 33: 249–256.
- Meier H.E.M. 2006. Baltic Sea climate in the late twenty-first century: a dynamical downscaling approach using two global models and two emission scenarios. *Climate Dynamics* 27: 39–68.
- Meier H.E.M., Hordoir R., Andersson H.C., Dieterich C., Eilola K., Gustafsson B.G., Höglund A. & Schimanke S. 2012. Modeling the combined impact of changing climate and changing nutrient loads on the baltic sea environment in an ensemble of transient simulations for 1961–2099. *Climate Dynamics* 39: 2421–2441.
- Rousset C., Vancoppenolle M., Madec G., Fichefet T., Flavoni S., Barthélemy A., Benshila R., Chanut J., Levy C., Masson S. & Vivier F. 2015. The Louvain-La-Neuve sea ice model LIM3.6: global and regional capabilities. *Geoscientific Model Development* 8: 2991–3005.
- Schimanke S., Dieterich C. & Meier H.E.M. 2014. An algorithm based on sea-level pressure fluctuations to identify major baltic inflow events. *Tellus A* 66: 23452, doi:10.3402/tellusa.v66.23452.
- TraFi 2010. *Ice class regulations 2010: “Finnish–Swedish Ice Class Rules 2010”*. TRAFI/31298/03.04.01.00/2010, Finnish Transport Safety Agency, Helsinki, Finland. [Available at http://www.trafi.fi/filebank/a/1328276403/5e67a19cb56529f0fbd531539e08438f9131-36441-Jaal-uokkamaaraykset_TRAFI_31298_03_04_01_00_2010_EN_corr_20_Dec_2010.pdf].
- Valdez-Banda O.A., Goerlandt F., Montewka J. & Kujala P. 2015. A risk analysis of winter navigation in finnish sea areas. *Accident Analysis & Prevention* 79: 100–116.
- Valdez-Banda O.A., Goerlandt F., Kuzmin V., Kujala P. & Montewka J. 2016. Risk management model of winter navigation operations. *Marine Pollution Bulletin* 108: 242–262.
- Vancoppenolle M., Fichefet T., Goosse H., Bouillon S., Madec G. & Morales-Maqueda M. 2009. Simulating the mass balance and salinity of Arctic and Antarctic sea ice. 1. Model description and validation. *Ocean Modelling* 27: 33–53.
- Vihma T. & Haapala J. 2009. Geophysics of sea ice in the baltic sea: a review. *Progress in Oceanography* 80: 129–148.

Appendix. LIM3 in Nemo-Nordic.

Specific tuning of LIM3 for Baltic and North Sea adaptation

Nemo-Nordic uses the LIM3 Ice Model (Vancoppenolle *et al.* 2009, and see http://www.climate.be/users/lecomte/LIM3_users_guide_2012.pdf) in its latest release (Rousset *et al.* 2015). Specific tuning was made in LIM3 to represent as well as possible the Baltic Sea sea ice dynamics. The purpose of this appendix is to present this tuning, and to provide a validation of the LIM3 implementation in Nemo-Nordic. The LIM3 model was used in its present form, but a few lines of code were added to parameterise fast ice. Tuning was also done only based on the possible changes given by the LIM3 namelist.

In addition to the description of the fast ice parameterisation in LIM3, we detail the changes which are made from the original options used for Nemo based global simulations (ORCA configurations) that include the Arctic ocean and/or the Antarctic sea ice.

Ice thermodynamics and salinity

Unlike most Nemo based configurations which include ice, LIM3 was not initialised with any ice cover as the ice melts totally during summertime in the Baltic Sea. Since all simulations started on 1 January, this approximation only affected the first year of the simulation, which was not used in any of the analysis afterwards anyway. The minimum thickness for ice formation was changed to 0.01 m to take into account the possible formation of thin ice in the Baltic Sea. The ice salinity in the Baltic Sea is very low, and that is why we chose not to use the prognostic option of ice salinity available in LIM3: the ice salinity in Nemo-Nordic was set to a constant value of 0.001 PSU, which corresponds to a 10th of the value of salinity set for river runoff (0.01 PSU), a value which is itself below the actual value of river salinity. This value for ice salinity was chosen because simply choosing zero salinity for sea ice results in instabilities in the ice model. Setting a value which is higher than the runoff value resulted in possible salinity instabilities in the ocean component, especially when sea ice is being created close to river input locations such as the Gulf of St. Petersburg or the Bothnian Bay, where the salinity is very low. Since the salinity was simply kept constant in the ice model, no salinity restoring nor any gravity drainage processes are used in Nemo-Nordic.

Sea-ice dynamics

Thickness distribution was discretised using five different categories with lower category limits: 0.0, 0.25, 0.56, 0.95 and 1.46 m. The ice dynamics uses a modified elastic-viscous-plastic (EVP) rheology (e.g. Bouillon *et al.* 2009) and accounts for sea-ice deformation processes (ridging and rafting).

The coastline of the Baltic Sea is very difficult to describe at the resolution of Nemo-Nordic used in the present simulations. Between the mainland and the open sea, there are archipelagos in many locations along the Swedish and Finnish coasts with countless islands and rocks whose dimensions are very often below what a 2-nautical-mile grid can resolve. However, the ice motion in such places is blocked by the islands, which ensures that no ice ridges can develop along the coasts sheltered by such archipelagos. Ice ridges usually develop further off the coasts where ice motion is enabled. In Nemo-Nordic, we included an ice velocity mask whose value was one for all sea points, except where the depth was lower than a value used as a tuning parameter, which in the present case was set to 15 m. In this latest case, the ice velocity mask was set to zero. Using this filter on ice drift velocities enabled blocking the ice drift in shallow areas, areas synonymous with the presence of an archipelago.

In addition to the fast ice parameterisation, tuning was made in the LIM3 namelist. The Baltic Sea produces thinner ice than the Arctic or the Antarctic, leading to a different tuning for the sea ice

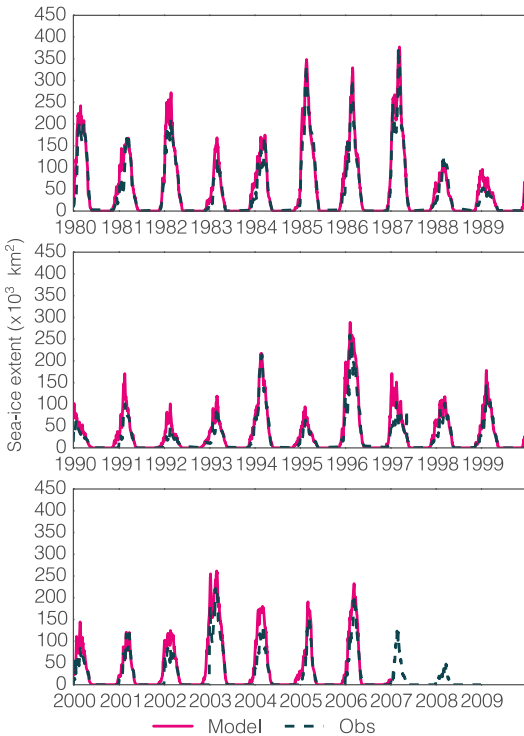


Fig. A1. Inter-annual and seasonal variability of sea-ice extent in Nemo-Nordic (model) and observations (obs).

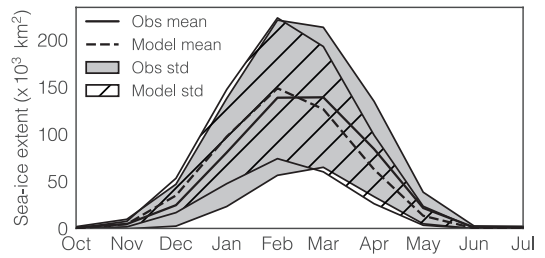


Fig. A2. Seasonal mean \pm standard deviation (std) sea-ice extent in Nemo-Nordic (dashed line and hatched area) and observations (solid line and grey area).

dynamics. The maximum thickness of ridged ice is 100 m in the global Nemo based configurations, this thickness was reduced to 30 m for the case of the Baltic Sea. In the same manner, the threshold thickness for ridging was reduced from 0.75 m to 0.07 m. The Nemo-Nordic grid has a higher resolution than that of global models, which enabled us to reduce dramatically the diffusivity of momentum of LIM3 from 350 m s^{-1} to 1 m s^{-1} .

Validation

The observational estimate of sea ice cover was based on ice charts from the Swedish Ice Service. The modelled total sea ice cover accurately described the seasonal and inter-annual variability (Fig. A1). There was, however, a slight bias in the seasonal cycle of freezing and melting (Fig. A2). Nemo-Nordic usually indicates freeze and melt too early in the ice season. The difference in thermal inertia of the model could be related to a bias in snow forcing. This bias was indeed noticed in the forcing.

The decadal trends were stronger in the observations than in the hindcast simulation (Fig. 3). A trend analysis of the annual maximum ice extent yields a simulated trend of -7 km/decade , for the 1961–2006 period, which is much lower than the observed trend of -36 km/decade (not shown). The lower simulated trend was mainly related to a bias in Kattegat and related to a bias in the downscaled ERA-40 temperature forcing. It is unclear whether this bias exists in the downscaled scenarios, nevertheless, the ice in the Kattegat region disappears in all future scenarios and will thus not affect our results.